

Fiber networks amplify active stress

Pierre Ronceray,^{1,*} Chase Broedersz,^{2,3,†} and Martin Lenz^{1,‡}

¹*Univ. Paris-Sud; CNRS; LPTMS; UMR 8626, Orsay 91405 France.*

²*Lewis-Sigler Institute for Integrative Genomics and Joseph Henry Laboratories of Physics, Princeton University, Princeton, NJ 08544, USA*

³*Arnold-Sommerfeld-Center for Theoretical Physics and Center for NanoScience, Ludwig-Maximilians-Universität München, Theresienstrasse 37, D-80333 München, Germany.*

Large-scale force generation is essential for biological functions such as cell motility, embryonic development, and muscle contraction. In these processes, forces generated at the molecular level by motor proteins are transmitted by disordered fiber networks, resulting in large-scale active stresses. While these fiber networks are well characterized macroscopically, this stress generation by microscopic active units is not well understood. Here we theoretically study force transmission in these networks, and find that local active forces are rectified towards isotropic contraction and strongly amplified as fibers collectively buckle in the vicinity of the active units. This stress amplification is reinforced by the networks' disordered nature, but saturates for high densities of active units. Our predictions are quantitatively consistent with experiments on reconstituted tissues and actomyosin networks, and shed light on the role of the network microstructure in shaping active stresses in cells and tissue.

Living systems constantly convert biochemical energy into forces and motion. In cells, forces are largely generated internally by molecular motors acting on the cytoskeleton, a scaffold of protein fibers (Fig. 1a). Forces from multiple motors are propagated along this fiber network, driving numerous processes such as mitosis and cell motility [1, 2], and allowing the cell as a whole to exert stresses on its surroundings. At the larger scale of connective tissue, many such stress-exerting cells act on another type of fiber network known as the extracellular matrix (Fig. 1b). This network propagates cellular forces to the scale of the whole tissue, powering processes such as wound healing [3] and morphogenesis [4]. Despite important differences in molecular details and length scales, a common physical principle thus governs stress generation in biological matter: internal forces from multiple localized “active units”—motors or cells—are propagated by a fiber network to generate large-scale stresses. However, a theoretical framework relating microscopic internal active forces to macroscopic stresses in these networks is lacking.

This generic stress generation problem is confounded by the interplay of network disorder and nonlinear elasticity. Active units generate forces at the scale of the network mesh size, and force transmission to larger scales thus sensitively depends on local network heterogeneities. In the special case of linear elastic networks, the macroscopic active stress is simply given by the density of active force dipoles, irrespective of network characteristics [5]. Importantly however, this relationship is not applicable to most biological systems, since typical active forces are

amplified sufficient to probe the nonlinear properties of their constitutive fibers, which stiffen under tension and buckle under compression [6]. Indeed, recent experiments on reconstituted biopolymer gels have shown that individual active units induce widespread buckling and stiffening [7–9], and theory suggests that such fiber nonlinearities can enhance the range of force propagation [10, 11].

Fiber networks also exhibit complex, nonlinear mechanical properties arising at larger scales, owing to collective deformations favored by the networks' weak connectivity [6, 12–14]. The role of connectivity in elasticity was famously investigated by Maxwell [15], who noticed that a spring network in dimension d becomes mechanically unstable for connectivities $z < 2d$. Interestingly, most biological fiber networks exhibit connec-

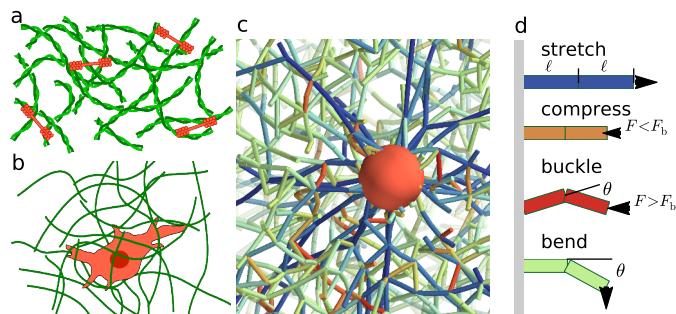


Figure 1. Biological fiber networks (green) transmit forces generated by localized active units (red). **a.** Myosin molecular motors exert forces on the actin cytoskeleton. **b.** Contractile cells exert forces on the extracellular matrix. **c.** The large nonlinear deformations induced by a model active unit in the surrounding fiber network result in stress amplification, as shown in this paper. See fiber color code in the next panel. **d.** Each bond in the network comprises two rigid segments hinged together to allow bending and buckling.

* pierre.ronceray@u-psud.fr

† c.broedersz@lmu.de

‡ martin.lenz@u-psud.fr

tivities well below this threshold, and therefore cannot be stabilized solely by the longitudinal stretching rigidity of their fibers. Instead, their macroscopic mechanical properties are typically controlled by the fiber bending rigidity [16]. In contrast to stretching-dominated networks with connectivities above the Maxwell threshold, such weakly connected, bending-dominated networks are soft and extremely sensitive to mechanical perturbations [16–19]. In these networks, stresses generated by active units propagate along intricate force chains [20, 21] whose effects on force transmission remain unexplored. Collections of such active units generate large stresses, with dramatic effects such as macroscopic network stiffening [22–24] and network remodelling [8, 9, 25–27].

Here we study the theoretical principles underlying stress generation by localized active units embedded in disordered fiber networks (Fig. 1c). We find that arbitrary local force distributions generically induce large isotropic, contractile stress fields at the network level, provided that the active forces are large enough to induce buckling in the network. In this case, the stress generated in a biopolymer network dramatically exceeds the stress level that would be produced in a linear elastic medium [5, 28], implying a striking network-induced amplification of active stress. Our findings elucidate the origins and magnitude of stress amplification observed in experiments on reconstituted tissues [7, 29] and actomyosin networks [22, 27, 30]. We thus provide a new conceptual framework for stress generation in biological fiber networks.

A LATTICE MODEL FOR ELASTIC FIBER NETWORKS

We investigate force transmission using a lattice-based fiber network model [16, 31]. In our model, straight fibers are connected at each lattice vertex by crosslinks that do not constrain their relative angles. Each lattice edge represents a “bond” made of two straight segments and can thus stretch, bend, or buckle (Fig. 1d). Segments have stretching rigidity μ and a rest length equal to one, implying a stretching energy $\mu(\ell - 1)^2/2$ per segment of length ℓ . The fiber bending rigidity is set to unity by penalizing angular deflections θ between consecutive segments through a bending energy $2\sin^2(\theta/2)$. Consequently, individual bonds buckle under a critical force $F_b = 1$, and we consider nearly inextensible fibers by assuming $\mu \gg 1$ (henceforth we use $\mu = 10^3$).

Network disorder is introduced through bond depletion, *i.e.*, by randomly decimating the lattice so that two neighboring vertices are connected by a bond with probability p . This probability controls the network’s connectivity, giving rise to distinct elastic regimes delimited by two thresholds p_{cf} and p_b . The network is stretching-dominated for $p > p_{cf}$, bending-dominated for $p_b < p < p_{cf}$, and mechanically unstable for $p < p_b$. Here we consider 2D hexagonal lattices, for which $p_b \simeq 0.45$

and $p_{cf} \simeq 0.65$, and 3D FCC lattices with $p_b \simeq 0.27$ and $p_{cf} \simeq 0.47$. Since the network displays singular behavior in the vicinity of p_b and p_{cf} , here we focus our investigations on the generic stretching- and bending-dominated regimes away from these critical points [16].

We model active units as sets of forces \mathbf{F}_i exerted on network vertices i with positions \mathbf{R}_i , and consider networks at mechanical equilibrium under the influence of these forces. We denote by σ the trace (*i.e.*, the isotropic component) of the coarse-grained active stress induced in the fiber network by a density ρ of such units.

The relationship between this active stress and local forces in homogeneous linear networks is very simple, and yields [5]

$$\sigma = \sigma_{\text{lin}} = -\rho \mathcal{D}_{\text{loc}}, \quad (1)$$

where $\mathcal{D}_{\text{loc}} = \sum_i \mathbf{F}_i \cdot \mathbf{R}_i$ is the dipole moment of the forces associated with a single active unit. Equation (1) is generically violated in disordered or nonlinear networks, although it holds on average in linear networks with homogeneous disorder:

$$\langle \sigma \rangle = \sigma_{\text{lin}}, \quad (2)$$

where $\langle \cdot \rangle$ denotes the average over disorder [5]. To quantify violations of Eq. (1), we define the far-field force dipole \mathcal{D}_{far} through the relation

$$\sigma = -\rho \mathcal{D}_{\text{far}} \quad \Rightarrow \quad \frac{\mathcal{D}_{\text{far}}}{\mathcal{D}_{\text{loc}}} = \frac{\sigma}{\sigma_{\text{lin}}}. \quad (3)$$

Conceptually, this far-field dipole characterizes the apparent strength of an individual active unit renormalized by force transmission in the disordered, nonlinear network. It quantifies how contractile ($\mathcal{D}_{\text{far}} < 0$) or extensible ($\mathcal{D}_{\text{far}} > 0$) the active medium is, and the dipole amplification ratio $\mathcal{D}_{\text{far}}/\mathcal{D}_{\text{loc}}$ (or equivalently the stress amplification ratio $\sigma/\sigma_{\text{lin}}$) measures the deviation from linear homogeneous force transmission.

CONTRACTILITY ROBUSTLY EMERGES FROM LARGE LOCAL FORCES

Stress generation by active units integrates mechanical contributions from a range of length scales. We first consider the immediate vicinity of the active unit. Network disorder plays a crucial role at that scale, since forces are transmitted through a random pattern of force lines determined by the specific configuration of depleted bonds (Fig. 2a-b). To understand how these patterns affect force transmission, we investigate the probability distribution of the far-field force dipole \mathcal{D}_{far} for simple active units consisting of two equal and opposite point forces of magnitude F_0 .

We first consider the linear regime $F_0 \ll F_b$, where the average dipole amplification equals unity: $\langle \mathcal{D}_{\text{far}}/\mathcal{D}_{\text{loc}} \rangle = 1$ [see Eqs. (2-3)]. The fluctuations around this average are strikingly broad, as shown in Fig. 2c. For instance, a

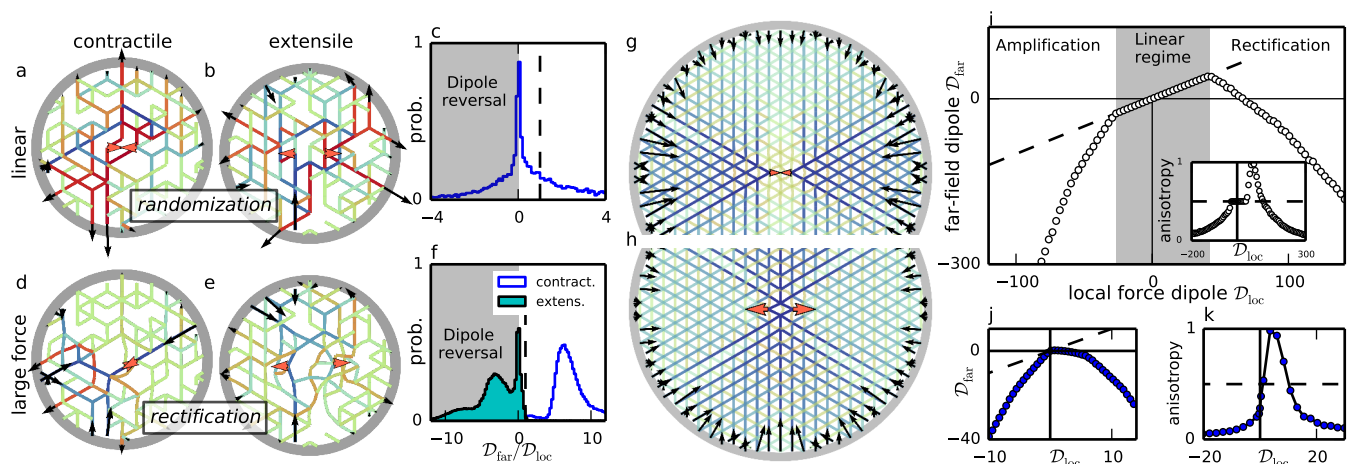


Figure 2. Network buckling converts active forces into emergent isotropic contraction over a few mesh sizes. **a-b**: In the linear response regime ($F_0 \ll F_b$), contractile and extensile active forces (red arrowheads) propagate along a complex network of force lines (blue=tension, red=compression), resulting in randomized force distributions at a fixed boundary (black arrows). **c**: The resulting distribution of dipole amplification ratios $\mathcal{D}_{\text{far}}/\mathcal{D}_{\text{loc}}$ is broad with widespread negative amplification (gray area) and an average equal to one (dashed line) ($n = 10^4$ samples). **d-e**: At larger forces (here $F_0 = 20F_b$), both contractile and extensile dipoles typically result in contractile forces at the boundary. **f**: Accordingly, the corresponding distribution of amplifications displays overwhelming negative amplification for locally extensile dipoles ($n = 10^4$ samples). **g-h**: Regular networks subjected to large ($F_0 = 500F_b$), local dipoles of either sign exert uniformly contractile forces on the fixed boundary. **i**: Corresponding far-field dipole as a function of the local dipole, showing amplification and rectification in the nonlinear regime. *Inset*: stress anisotropy parameter $1 - (\sum_{\mu} \sigma^{\mu\mu})^2 / (d \sum_{\mu,\nu} \sigma^{\mu\nu} \sigma^{\nu\mu})$, as a function of the local dipole. Here $\sigma^{\mu\nu}$ is the coarse-grained active stress tensor of the active medium (see Supporting Information). **j-k**: Far-field dipole and anisotropy as a function of the local dipole in a bending-dominated 2D network ($p = 0.6$, averaged over $n = 10^4$ samples).

significant fraction (37%) of all network geometries yield negative amplification, *i.e.*, an effective extensility in response to a contractile dipole (Fig. 2b). Overall, the far-field response in the linear regime is only loosely correlated to the applied force dipole.

The situation is dramatically different in the large force regime ($F_0 \gg F_b$), where fibers buckle and induce nonlinear network response. This is illustrated by the distributions of dipole amplifications in two opposite cases: a large contractile and a large extensile force dipole (Fig. 2d-f). First, locally extensile dipoles predominantly undergo negative amplification, implying far-field contractility irrespective of the sign of \mathcal{D}_{loc} (as in, *e.g.*, Fig. 2e). Second, the randomization observed in the linear regime is strongly attenuated, and the sign of the amplification is very reproducible (positive for 98% of the contractile dipoles and negative for 86% of the extensile ones). Third, the magnitude of the average amplification is significantly larger than one (in Fig. 2f $\langle \mathcal{D}_{\text{far}}/\mathcal{D}_{\text{loc}} \rangle = 6.9$ and -3.2 for contractile and extensile dipoles, respectively).

To understand these three effects, we consider contractile and extensile dipoles in a simpler regular network (no bond depletion, Fig. 2g-h). Qualitatively, these uniform networks behave similarly to the randomly depleted ones described above: force dipole conservation holds for $F_0 \ll F_b$, while for $F_0 \gg F_b$ dipoles are rectified towards contraction and their magnitude is amplified (Fig. 2i). The origin of these behaviors is apparent

from the spatial arrangement of the forces in Figs. 2g-h. While contractile and extensile active units both induce compressive and tensile stresses in their immediate surroundings, the buckling of the individual bonds prevents the long-range propagation of the former. This results in enhanced tensile stresses in the far-field, and thus in strongly contractile far-field dipoles. In addition, this nonlinear response renders the far-field stresses uniformly tensile, and therefore more isotropic than the active unit forces. We quantify this effect in the inset of Fig 2i using an anisotropy parameter for the far-field stresses, which indeed becomes very small for both positive or negative large local dipoles.

Moving to a systematic quantification of force transmission in depleted, bending-dominated networks, we show in Fig 2j-k the same three effects of rectification, amplification and isotropization, which set in at smaller forces than in regular networks. Overall, these effects are very general and hold in both bending- and stretching-dominated depleted networks, in two and three dimensions, and for active units with complicated force distributions (see supporting Figs. S3 and S4). Thus, beyond the immediate neighborhood of the active force-generating unit, strong isotropic contractile stresses emerge in the system from a generic local force distribution due to the nonlinear force propagation properties of the fiber network.

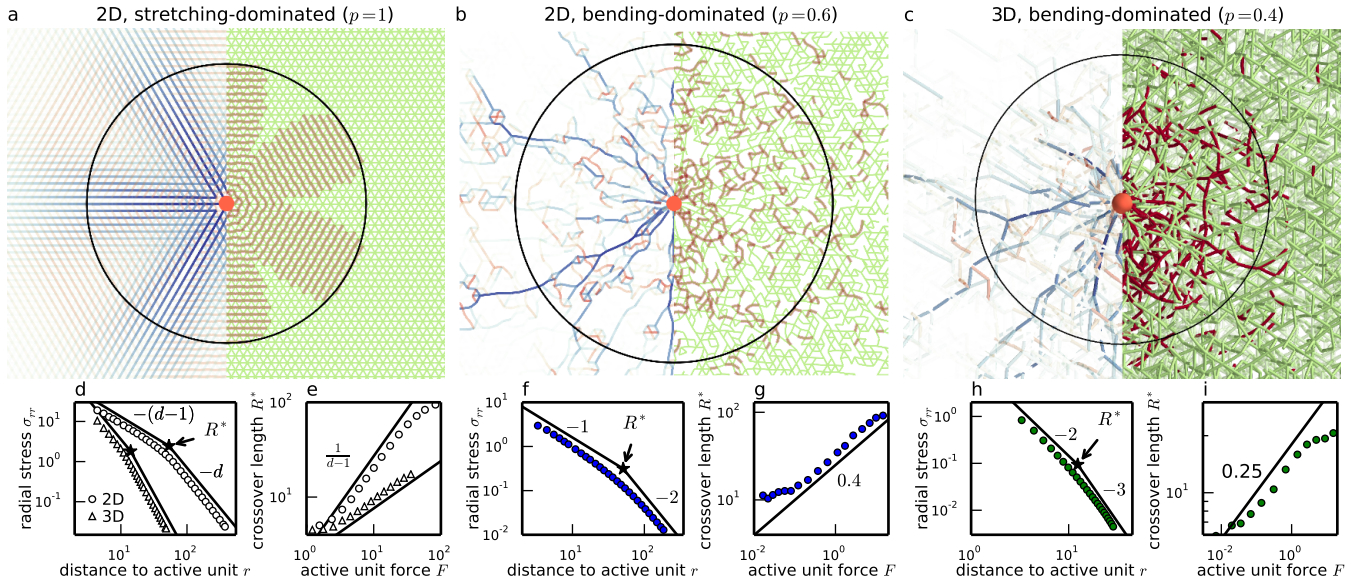


Figure 3. Nonlinear network behavior enhances the range over which stresses are transmitted. **a-c**: A localized, isotropically pulling active unit (red circle of radius $R_0 = 1.95$) induces stress lines (left side of each panel, blue=tension and red=compression) and buckling (right side of each panel, in red; non-buckled bonds are green) in the surrounding fiber network. Black circle: radius R^* of the rope-like region. Panel **c** shows a slice of a 3D system. **d, f** and **h**: Decay of the average radial stress in the network (corrected for boundary effects, see Supporting Information) as a function of the distance to the active unit. Fitting the curve with the power laws of Eqs. (5-6) yields a measure of the crossover radius R^* . **e, g** and **i**. We tentatively describe the dependence of the crossover radius on active unit force by a power law (solid line) in the intermediate- F regime where it is not complicated by finite size effects due to either the active unit size (at small F) or that of the system boundary (at large F). Results obtained in a 2D circular (3D spherical) network of radius 200 (33) with fixed boundaries and averaged over 100 samples for disordered networks.

A MODEL FOR ACTIVE UNITS AS ISOTROPIC PULLERS

While nonlinear force transmission over large length scales involves large active forces, the model for active units used above can only exert moderate dipoles in soft, weakly connected networks. Indeed, for large enough contractile dipoles the two vertices on which the forces are applied collapse to a point (Fig. 2d), preventing further contraction. In contrast, molecular motors and contractile cells continuously pull fibers in without collapsing. To reflect this, we introduce an active unit capable of exerting arbitrarily large forces without changing its size. The unit is centered on a vertex i , and pulls on any vertex j within a distance $2R_0$ with a radial force

$$\mathbf{F}_{ij} = \begin{cases} -F_0 \frac{r_{ij}}{R_0} \hat{\mathbf{r}}_{ij} & \text{if } r_{ij} < R_0 \\ -F_0 \left(2 - \frac{r_{ij}}{R_0}\right) \hat{\mathbf{r}}_{ij} & \text{if } R_0 \leq r_{ij} < 2R_0 \end{cases}, \quad (4)$$

where F_0 is the maximum force exerted by the unit on a vertex, r_{ij} is the distance between i and j and $\hat{\mathbf{r}}_{ij}$ is the associated unit vector. A strong active unit in a soft network may pull in many fibers, exerting a force $\approx F_0$ on each of them. Adding the contributions of all these fibers results in a large local dipole, the magnitude of which is not well reflected by the value of F_0 . The influence of the active unit on the surrounding network is better characterized by the force F , which we define as the average

force per unit area exerted on the surrounding network by the active unit at its outer surface ($r = 2R_0$). Finally, we assign an isotropic force distribution to the active puller defined in Eq. (4). This choice is justified by the observation that anisotropic force distributions are rectified towards isotropy by the network (Figs. 2i, k).

CONTRACTILE FORCES ARE LONG-RANGED IN BUCKLABLE MEDIA

We now study force propagation beyond the immediate vicinity of an active unit (Fig. 3) using the above-described isotropic puller. Simple theoretical arguments dictate two asymptotic regimes for this propagation. Close to the active unit, forces are large and fiber buckling affects force transmission, while beyond a crossover distance R^* forces are weak and linear elasticity prevails.

To describe the near-field regime, we note that fiber buckling prevents the network from sustaining compressive stresses above the buckling threshold. Close to the active unit, the network is thus effectively equivalent to a network of floppy ropes. The active unit pulls on these ropes, and thus becomes the center of a radial arrangement of tensed ropes. Force balance on a small portion of a spherical shell centered on the active unit imposes

that radial stresses in this rope-like medium decay as

$$\sigma_{rr}(r) \propto r^{-(d-1)}, \quad r < R^* \quad (5)$$

where r is the distance from the active unit and d the dimension of space [32]. In the far field, stresses are small and buckling does not occur, implying that force transmission crosses over from rope-like to linear elasticity:

$$\sigma_{rr}(r) \propto r^{-d}, \quad r > R^*. \quad (6)$$

Stress decay is thus significantly slower in the rope-like near-field than in the linear far-field, leading to an increased range for force transmission [11]. Conceptually, the faster decay in a linear elastic medium can again be understood by balancing forces on a fraction of spherical shell centered on the active unit, where radial stresses are now partially compensated by orthoradial stresses. We expect that the crossover between these two regimes occurs when radial stresses are comparable to the buckling stress, implying that the crossover length depends on the active force:

$$R^* \approx R_0 \left(\frac{F}{F_b} \right)^{1/(d-1)} \quad (7)$$

To test this two-regime scenario, we simulate force propagation away from a single active unit in both stretching- and bending-dominated networks in two and three dimensions. In all cases, rope-like radial stresses and bond buckling are predominant in the vicinity of the active unit (Fig. 3a-c). Monitoring the decay of radial stresses with r , we find an apparent crossover from rope-like to linear behavior, consistent with Eqs. (5) and (6) (Fig. 3d, f, h).

Visually, the crossover length R^* coincides with the outer boundary of the radially tensed, buckling-rich region (Fig. 3a-c, black circles). In stretching-dominated networks, our prediction of Eq. (7) captures the force dependence of this crossover length (Fig. 3e and S5). In contrast, bending-dominated networks display a more complex behavior: while the system still exhibits a transition from rope-like to linear force transmission, the crossover region is much broader (Fig. 3f, h) and forces propagate along heterogeneous patterns reminiscent of previously reported force chains (Fig. 3b-c) [20, 33]. This strong concentration of the tensile stresses allows rope-like force transmission to extend much further than predicted by Eq. (7). Instead, we find behavior that is reasonably well described by a power law $R^* \propto F^\alpha$ with anomalous exponents $\alpha \approx 0.4$ in 2D and $\alpha \approx 0.25$ in 3D (Fig. 3g, i). These exponents appear to be insensitive to the exact value of the depletion parameter p within the bending-dominated regime (Supporting Fig. S5). The difference between stretching- and bending-dominated exponents suggests elastic heterogeneities qualitatively affect force transmission in such soft networks. As a result, contractile forces large enough to induce buckling benefit from an enhanced range of transmission, characterized by the mesoscopic radius of the rope-like region R^* .

AMPLIFICATION BY A COLLECTION OF ACTIVE UNITS

Over large length scales, active stresses in biological systems are generated by multiple active units. We thus compute the stress amplification ratio in the presence of a finite density of randomly positioned active units in 2D and 3D for various densities ρ and depletion parameters p (Fig. 4a). In all cases we observe three stress amplification regimes as a function of the unit force F : a low-force plateau without amplification, an intermediate regime of increasing amplification and a saturation of the amplification at a level that depends on ρ .

In the low-force regime, linear force transmission prevails (Fig. 4b) and the active stress is given by Eq. (1):

$$\sigma = \sigma_{\text{lin}} = -\rho \mathcal{D}_{\text{loc}} \approx \rho F R_0. \quad (8)$$

For moderate forces, the fibers in the network buckle in the vicinity of each active unit, up to a distance R^* . Individual units are thus typically surrounded by *nonoverlapping* nonlinear regions of size R^* , as illustrated in Fig. 4c. To predict the resulting active stress in the system, we model each nonlinear region as an effective active unit of size R^* and force dipole $\mathcal{D}_{\text{eff}} \approx -FR^*$, where we used Eq. (5) to describe force propagation within the nonlinear region. As the effective units are themselves embedded in a linear medium, linear force transmission [Eq. (1)] outside of these units implies

$$\sigma \approx -\rho \mathcal{D}_{\text{eff}} \approx \rho F R^*. \quad (9)$$

We thus predict that stress amplification in this regime scales as $\sigma/\sigma_{\text{lin}} \approx R^*/R_0$. We confirm this prediction in Fig. 4e. Since R^* increases with the active unit force in this regime, the large-scale stress amplification $\sigma/\sigma_{\text{lin}}$ increases with F as previously observed in Fig. 4a.

For large forces, the radius of the rope-like regions becomes so large as to exceed the typical distance between adjacent active units $R_{\text{a.u.}} = \rho^{-1/d}$. This causes the nonlinear regions associated to neighboring active units to overlap, and renders the whole network mechanically equivalent to a collection of tensed, inextensible ropes whose geometry does not change significantly upon further increase of the force. To estimate the resulting network stress, we approximate the system as a mosaic of effective active units of size $R_{\text{a.u.}}$ each with a force dipole $\mathcal{D}_{\text{eff}} \approx -FR_{\text{a.u.}}$ (Fig. 4d). This yields

$$\sigma \approx -\rho \mathcal{D}_{\text{eff}} \approx \rho F R_{\text{a.u.}} = \rho^{1-1/d} F. \quad (10)$$

The resulting prediction for the stress amplification, $\sigma/\sigma_{\text{lin}} \approx R_{\text{a.u.}}/R_0$, is confirmed in Fig. 4f. Strikingly, the stress generated in this large-force regime has a non-linear dependence on ρ , again consistent with Fig. 4a. Indeed, the addition or removal of active units leads to large rearrangements of the rope network, resulting in significant local modifications of force transmission.

We summarize the physics of collective stress-generation by many active units in a phase diagram

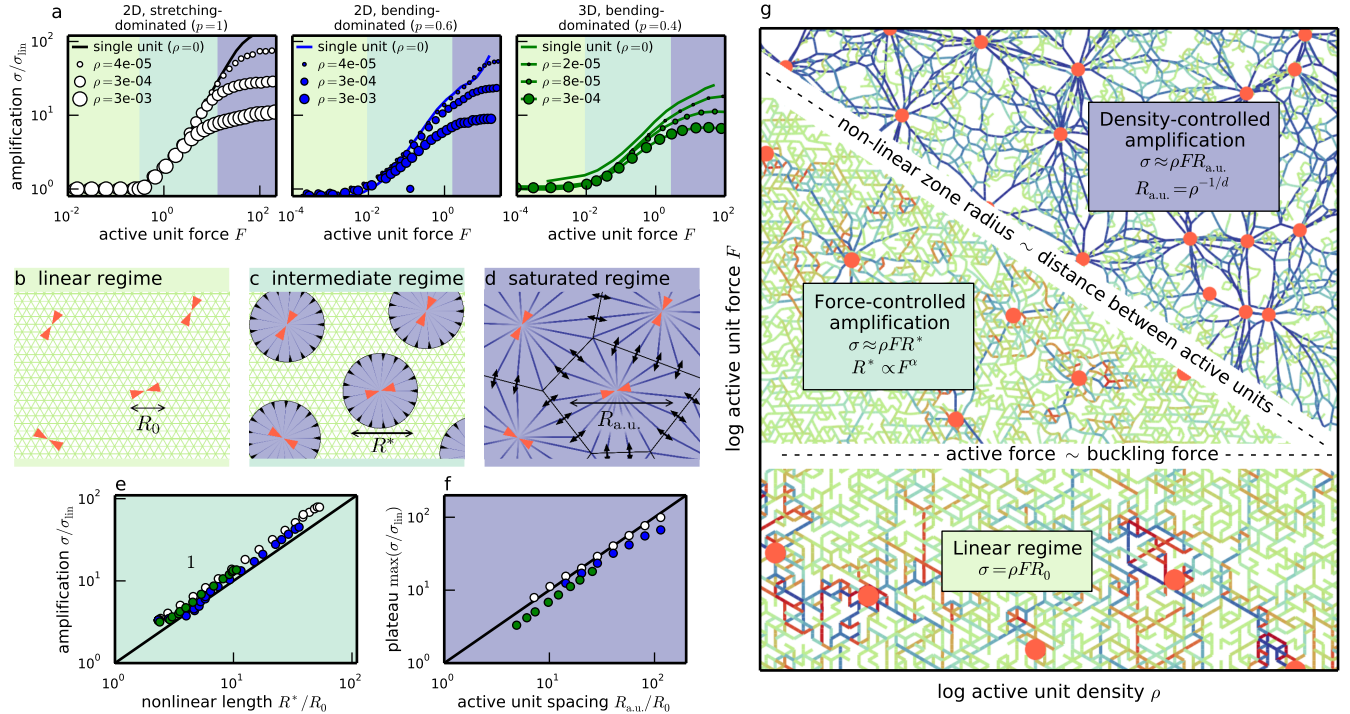


Figure 4. Force transmission in the presence of a finite density ρ of active units. **a.** Fiber networks in different dimensions and elastic regimes all display three stress amplification regimes as a function of active unit density and force, as suggested by the colored background. **b-d.** Schematics of the network structure in each regime. The low-force linear regime (**b.**) transitions to a regime of nonoverlapping nonlinear regions (**c.**) as soon as F is sufficient to induce buckling. These nonlinear regions grow with increasing F , and amplification saturates as they start overlapping, which turns the whole network into a rope network (**d.**). **e.** In the intermediate force regime, the stress amplification ratio is equal to the ratio R^*/R_0 as predicted by Eq. (9). **f.** In the large-force regime, the stress amplification ratio is equal to the ratio $R_{a.u.}/R_0$ as predicted by Eq. (10). **g.** Schematic phase diagram indicating the domain of applicability of the three stress amplification regimes, with representative snapshots of the corresponding systems in the background.

(Fig. 4g). In each regime, the magnitude of an active unit's effective force dipole is directly proportional to one of the three length scales R_0 , R^* and $R_{a.u.}$ [Eqs. (8-10)]. While we have shown that R^* depends on the dimensionality and connectivity of the network, the other two length scales are purely geometrical. An important consequence of these findings is that the active stress generated in the associated regimes is essentially independent of the detailed properties of the fiber network.

DISCUSSION

In living organisms, microscopic units exert active forces that are transmitted by fibrous networks to generate large-scale stresses. The challenge in analyzing this force-transmission problem stems from the disordered architecture of such fibrous networks and the nonlinearities associated with the strong forces exerted by biological active units. Despite this complexity, we find surprisingly simple and robust behaviors: in response to any distribution of active forces, dramatically amplified contractile stresses emerge in the network on large scales. This re-

markable property hinges only on the local asymmetry in elastic response between tensed and compressed fibers, and is enhanced by network disorder. Our simple, yet realistic description of individual fibers yields a universal scenario for force transmission: long-ranged, rope-like propagation near a strong active unit, and linear transmission in the far-field. This generic result should be contrasted with recent studies focused on fibers with special singular force-extension relation [11, 32] and resulting in non-universal force transmission regimes.

Our generic phase diagram (Fig 4g) recapitulates our quantitative understanding of stress generation by a collection of active units based on the interplay between three length scales: active unit size R_0 , rope-like length R^* , and typical distance between units $R_{a.u.}$. To validate these predictions, we compare them with existing measurements on a broad range of *in vitro* systems (Table I). We first consider system I, a dense three-dimensional actin network with mesh size $\simeq 200$ nm in the presence of myosin motors, which assemble into so-called myosin thick filaments. A thick filament—which we consider as an individual active unit—exerts a typical force $F = 6$ pN, much smaller than the buckling thresh-

Table I. Experimental data support stress amplification in fiber networks. The rope-like radius R^* , linear-theory active stress σ_{lin} and predicted amplified stress σ_{th} are computed using Eqs. (8-10) from independent estimates of the single-unit force F (see Supporting Information) for comparison with the experimentally measured active stress σ_{exp} . We use the stretching-dominated scaling for R^* [Eq. (7)], and thus the predicted active stress in system II is a lower bound as indicated by the “ \geq ” symbol in the σ_{th} column; the “ \geq ” in the σ_{exp} column reflects experimental uncertainties.

System	R_0	R_{au}	$R^* = R_0(F/F_b)^{1/(d-1)}$	σ_{lin}	σ_{th}	σ_{exp}
I 3D actomyosin [22]	$1 \mu\text{m}$	$1 \mu\text{m}$	$0.3 \mu\text{m}$ (linear regime)	12 Pa	12 Pa	14 Pa
II 2D actomyosin [27, 30]	$1 \mu\text{m}$	$20 \mu\text{m}$	$15 \mu\text{m}$ (force-controlled)	$0.014 \text{ pN}/\mu\text{m}$	$\geq 0.2 \text{ pN}/\mu\text{m}$	$\geq 1 \text{ pN}/\mu\text{m}$
III 3D blood clot [7, 29]	$2 \mu\text{m}$	$15 \mu\text{m}$	$70 \mu\text{m}$ (density-controlled)	9 Pa	70 Pa	150 Pa

old $F_b \approx 50 \mu\text{m}$ associated with a single 200 nm-bond. This implies an active stress identical to the linear prediction, as confirmed by the experimental result [22]. We next consider system II, a two-dimensional actin network bound to the outer surface of a lipid vesicle. The active units are essentially the same as in System I, but are much more sparsely distributed ($R_{\text{a.u.}} \simeq 20 \mu\text{m}$). The network in system II is also much looser (mesh size $\simeq 1 \mu\text{m}$) than in system I, resulting in a much smaller bond buckling force. The combination of a low buckling threshold and a large spacing between active units leads us to predict a significant stress amplification $R^*/R_0 \simeq 15$ associated to the force-controlled regime (Fig 4c, g), in reasonable agreement with experiments [27, 30]. Finally, we consider a clot comprised of fibrin filaments and contractile platelets as active units (system III). The large forces exerted by platelets allow for long-range nonlinear effects, placing this *in vitro* system deep in the density-controlled regime (Figs. 4d, g). Consequently, we expect stress amplification to be controlled by the distance between active units, irrespective of the large value of the active force $F \approx 10^5 F_b$. We thus predict an amplification factor $R_{\text{a.u.}}/R_0 \simeq 8$, in good agreement with experimental data [7, 29]. These three examples demonstrate our theory’s ability to quantitatively account for stress amplification, and recent progress in the micromechanical characterization of active fiber networks opens promising perspectives for further exploring active stress amplification [7, 9, 27].

Far from merely transmitting active forces, we show that fiber networks dramatically alter force propagation as contractility emerges from arbitrary spatial distributions of local active forces. This could imply that living organisms do not have to fine-tune the detailed geometry of their active units, since any local force distribution yields essentially the same effects on large length scales. This emergence of contractility sheds a new light on the longstanding debate in cytoskeletal mechanics regarding the emergence of macroscopic contraction in non-muscle actomyosin despite the absence of an intrinsic contractility of individual myosin motors [33–38]. Indeed, while these motors exert equal amounts of local pushing and pulling forces [39, 40], our result suggests that the surrounding network rectifies pushing contributions into uniform contraction. More broadly, we suggest that this strong propensity for the emergence of contraction in fibrous materials can explain the overwhelming dominance

of contractile stresses in active biological materials up to the tissue level. Clearly, this does not mean that it is impossible to generate large-scale expansion in living organisms as required for limb abduction and extension or for lung inflation. Nevertheless, in each of these examples the expansion actually results from the clever harnessing of muscle contraction through lever structures involving our skeleton.

Our results suggest a novel design principle for active fiber networks geared to maximize stress-generation. In a linear medium, the stress generated does not depend on the spatial distribution of active units. In contrast, we predict that in fiber networks, larger stresses can be obtained by clustering the active units. Such regrouping of a set number of force generators to enhance stress amplification could play a role in smooth muscle, where the number of myosins in individual thick filament is regulated dynamically [41]. Similarly, at the tissue level, clustering of contractile cells occurs during wound repair [42].

Our findings connect widely used “active gels” phenomenological theories [43] to their underlying molecular foundation, a crucial step in bringing theory and experiments together in the study of active biological matter, and calls for further progress in characterizing force transmission in more complex fiber networks. Finally, beyond biopolymer networks our work opens avenues to understand force transmission in novel metamaterials whose macroscopic properties crucially hinge on their microscopic buckling [44, 45].

ACKNOWLEDGMENTS

We thank Cécile Sykes and Guy Atlan for fruitful discussions. This work was supported by grants from Université Paris-Sud and CNRS, the University of Chicago FACCTS program, Marie Curie Integration Grant PCIG12-GA-2012-334053 and “Investissements d’Avenir” LabEx PALM (ANR-10-LABX-0039-PALM) to ML as well as the German Excellence Initiative via the program ‘NanoSystems Initiative Munich’ (NIM) and the Deutsche Forschungsgemeinschaft (DFG) via project B12 within the SFB 1032. PR is supported by “Initiative Doctorale Interdisciplinaire 2013” from IDEX Paris-Saclay, and CPB is supported by a Lewis-Sigler fellowship. ML’s group belongs to the CNRS consortium CellTiss. Figures realized with Matplotlib [46] and

-
- [1] L. Blanchoin, R. Boujemaa-Paterski, C. Sykes, and J. Plastino, *Physiol. Rev.* **94**, 235 (2014).
- [2] D. A. Fletcher and R. D. Mullins, *Nature* **463**, 485 (2010).
- [3] H. P. Ehrlich, *Eye* **2**, 149 (1988).
- [4] C.-P. Heisenberg and Y. Bellaïche, *Cell* **153**, 948 (2013).
- [5] P. Ronceray and M. Lenz, *Soft Matter* **11**, 1597 (2015).
- [6] C. P. Broedersz and F. C. MacKintosh, *Rev. Mod. Phys.* **86**, 995 (2014).
- [7] W. A. Lam, O. Chaudhuri, A. Crow, K. D. Webster, T.-D. Li, A. Kita, J. Huang, and D. A. Fletcher, *Nat. Mater.* **10**, 61 (2011).
- [8] M. Soares e Silva, M. Depken, B. Stuhmann, M. Korsten, F. C. Mackintosh, and G. H. Koenderink, *Proc. Natl. Acad. Sci. U.S.A.* **108**, 9408 (2011).
- [9] M. Murrell and M. L. Gardel, *Proc. Natl. Acad. Sci. U.S.A.* **109**, 20820 (2012).
- [10] Y. Shokef and S. A. Safran, *Phys. Rev. Lett.* **108**, 178103 (2012).
- [11] J. Notbohm, A. Lesman, P. Rosakis, D. A. Tirrell, and G. Ravichandran, *Interface* **12**, 20150320 (2015).
- [12] P. R. Onck, T. Koeman, T. van Dillen, and E. van der Giessen, *Phys. Rev. Lett.* **95**, 178102 (2005).
- [13] C. Heussinger, B. Schaefer, and E. Frey, *Phys. Rev. E* **76**, 031906 (2007).
- [14] E. Conti and F. C. MacKintosh, *Phys. Rev. Lett.* **102**, 088102 (2009).
- [15] J. C. Maxwell, *Philos. Mag.* **27**, 294 (1864).
- [16] C. P. Broedersz, X. Mao, T. C. Lubensky, and F. C. MacKintosh, *Nat. Phys.* **7**, 983 (2011).
- [17] S. Ulrich, N. Upadhyaya, B. van Opheusden, and V. Vitelli, *Proc. Natl. Acad. Sci. U.S.A.* **110**, 20929 (2013).
- [18] M. Wyart, H. Liang, A. Kabla, and L. Mahadevan, *Phys. Rev. Lett.* **101**, 215501 (2008).
- [19] M. Sheinman, C. P. Broedersz, and F. C. MacKintosh, *Phys. Rev. Lett.* **109**, 238101 (2012).
- [20] C. Heussinger and E. Frey, *Eur. Phys. J. E* **24**, 47 (2007).
- [21] D. A. Head, A. J. Levine, and F. C. MacKintosh, *Phys. Rev. E* **72**, 061914 (2005).
- [22] G. H. Koenderink, Z. Dogic, F. Nakamura, P. M. Bendix, F. C. MacKintosh, J. H. Hartwig, T. P. Stossel, and D. A. Weitz, *Proc. Natl. Acad. Sci. U.S.A.* **106**, 15192 (2009).
- [23] K. A. Jansen, R. G. Bacabac, I. K. Piechocka, and G. H. Koenderink, *Biophys. J.* **105**, 2240 (2013).
- [24] C. P. Broedersz and F. C. MacKintosh, *Soft Matter* **7**, 3186 (2011).
- [25] P. M. Bendix, G. H. Koenderink, D. Cuvelier, Z. Dogic, B. N. Koeleman, W. M. Briehner, C. M. Field, L. Mahadevan, and D. A. Weitz, *Biophys. J.* **94**, 3126 (2008).
- [26] S. Köhler, V. Schaller, and A. R. Bausch, *Nat. Mater.* **10**, 462 (2011).
- [27] K. Carvalho, F.-C. Tsai, E. Lees, R. Voituriez, G. H. Koenderink, and C. Sykes, *Proc. Natl. Acad. Sci. U.S.A.* **110**, 16456 (2013).
- [28] J. Ranft, M. Basan, J. Elgeti, J.-F. Joanny, J. Prost, and F. Jülicher, *Proc. Natl. Acad. Sci. U.S.A.* **107**, 20863 (2010).
- [29] C. J. Jen and L. V. McIntire, *Cell Motil.* **2**, 445 (1982).
- [30] J. Lemièrre, M. Bussonnier, T. Betz, C. Sykes, and K. Carvalho, “Cell-sized liposome doublets reveal active cortical tension build up,” (2015), to appear.
- [31] M. Das, F. C. MacKintosh, and A. J. Levine, *Phys. Rev. Lett.* **99**, 038101 (2007).
- [32] P. Rosakis, J. Notbohm, and G. Ravichandran, *arXiv*, 1412.2612 (2014).
- [33] N. L. Dasanayake, P. J. Michalski, and A. E. Carlsson, *Phys. Rev. Lett.* **107**, 118101 (2011).
- [34] S. Hatano, *Int. Rev. Cytology* **156**, 199 (1994).
- [35] K. Sekimoto and H. Nakazawa, “Current topics in physics,” (World Scientific, Singapore, 1998) pp. 394–405.
- [36] M. Lenz, T. Thoresen, M. L. Gardel, and A. R. Dinner, *Phys. Rev. Lett.* **108**, 238107 (2012).
- [37] D. Mizuno, C. Tardin, C. F. Schmidt, and F. C. Mackintosh, *Science* **315**, 370 (2007).
- [38] M. Murrell, P. W. Oakes, M. Lenz, and M. L. Gardel, *Nat. Rev. Mol. Cell Biol.* (2015), 10.1038/nrm4012, advance online article doi:10.1038/nrm4012.
- [39] M. Lenz, M. L. Gardel, and A. R. Dinner, *New J. Phys.* **14**, 033037 (2012).
- [40] M. Lenz, *Phys. Rev. X* **4**, 041002 (2014).
- [41] C. Y. Seow, *Am. J. Physiol.-Cell Physiol.* **289**, C1363 (2005).
- [42] B. da Rocha-Azevedo and F. Grinnell, *Exp. Cell Res.* **319**, 2440 (2013).
- [43] J. Prost, F. Jülicher, and J.-F. Joanny, *Nat. Phys.* **11**, 111 (2015).
- [44] S. H. Kang, S. Shan, W. L. Noorduin, M. Khan, J. Aizenberg, and K. Bertoldi, *Adv. Mater.* **25**, 3380 (2013).
- [45] B. Florijn, C. Coulais, and M. van Hecke, *Phys. Rev. Lett.* **113**, 175503 (2014).
- [46] J. D. Hunter, *Comput. Sci. Eng.* **9**, 90 (2007).
- [47] P. Ramachandran and G. Varoquaux, *Comput. Sci. Eng.* **13**, 40 (2011).
- [48] F. Jülicher, K. Kruse, J. Prost, and J.-F. Joanny, *Phys. Rep.-Rev. Sec. Phys. Lett.* **449**, 3 (2007).
- [49] J.-F. Joanny and J. Prost, *HFSP J.* **3**, 94 (2009).
- [50] S. S. Rosenfeld, J. Xing, L.-Q. Chen, and H. L. Sweeney, *J. Biol. Chem.* **278**, 27449 (2003).
- [51] C. Storm, J. J. Pastore, F. C. MacKintosh, T. C. Lubensky, and P. A. Janmey, *Nature* **435**, 191 (2005).